Case Studies in Thermal Engineering 4 (2014) 32–41

Contents lists available at ScienceDirect

Case Studies in Thermal Engineering

journal homepage: www.elsevier.com/locate/csite

Heat transfer augmentation using nanofluids in an elliptic annulus with constant heat flux boundary condition

H.K. Dawood [a,b,*], H.A. Mohammed [c,**], K.M. Munisamy [a]

[a] Department of Mechanical Engineering, College of Engineering, Universiti Tenaga Nasional, Jalan IKRAM-UNITEN, 43009 Kajang, Selangor, Malaysia
[b] Department of Mechanical Engineering, College of Engineering, University of Anbar, Ramadi, Anbar, Iraq
[c] Department of Thermofluids, Faculty of Mechanical Engineering, Universiti Teknologi Malaysia, 81310 UTM Skudai, Johor Bahru, Malaysia

ARTICLE INFO

Article history:
Received 30 March 2014
Received in revised form
5 June 2014
Accepted 5 June 2014
Available online 13 June 2014

Keywords:
Mixed convection
Numerical modeling
Annulus
Heat transfer enhancement
Nanofluids

ABSTRACT

This work reports numerical simulation for three dimensional laminar mixed convective heat transfers at different nanofluids flow in an elliptic annulus with constant heat flux. A numerical model is carried out by solving the governing equations of continuity, momentum and energy using the finite volume method (FVM) with the assistance of SIMPLE algorithm. Four different types of nanofluids Al_2O_3, CuO, SiO_2 and ZnO, with different nanoparticles size 20, 40, 60 and 80 nm, and different volume fractions ranged from 0% to 4% using water as a base fluid were used. This investigation covers a Reynolds number in the range of 200 to 1000. The results revealed that SiO_2–Water nanofluid has the highest Nusselt number, followed by Al_2O_3–Water, ZnO–Water, CuO–Water, and lastly pure water. The Nusselt number increased as the nanoparticle volume fraction and Reynolds number increased; however, it decreased as the nanoparticle diameter increased. It is found that the glycerine–SiO_2 shows the best heat transfer enhancement compared with other tested base fluids.

1. Introduction

The heat transfer is a discipline of thermal engineering that concerns the generation, use, conversion, and exchange of thermal energy and heat between physical systems. Heat transfer is classified into various mechanisms, such as conduction, convection, and radiation. Convection is one of the major modes of heat transfer that can be qualified in terms of being natural, forced, gravitational, granular, or thermomagnetic. A combined model of natural and forced convection heat transfer can be classified as mixed convection heat transfer. Mixed convection heat transfer exists when natural convection currents are the same order of magnitude as forced flow velocities. The term “Combined Convection” is also used, and the flows may be internal or external to a bounding surface [1].

Mixed convection heat transfer and fluid flow in an annulus is a significant phenomenon in engineering systems as it is a common and essential geometry for fluid flow and heat transfer devices. It has a lot of engineering applications such as in double pipe heat exchanger, gas turbines, nuclear reactors, turbo machinery, thermal storage systems, aircraft fuselage insulation to underground electrical transmission cables, solar energy systems, boilers, cooling of electronic devices, compact heat exchangers, cooling core of nuclear reactors, cooling systems, gas-cooled electrical cables, thermal insulation,

* Corresponding authors at: Department of Mechanical Engineering, College of Engineering, Universiti Tenaga Nasional, Jalan IKRAM-UNITEN, 43009 Kajang, Selangor, Malaysia. Tel.: +60 7 55 34 716; fax: +60 7 55 66159.
** Corresponding author.
E-mail addresses: hathim_iraq@yahoo.com (H.K. Dawood), hussein.dash@yahoo.com (H.A. Mohammed).

http://dx.doi.org/10.1016/j.csite.2014.06.001

electrical gas insulated transmission lines ventilation and air conditioning system [2]. The heat transfer enhancement technology has been improved and widely used in the heat exchanger applications. One of the widely used heat transfer enhancement technique is inserting different shaped elements with different geometries in channel flow [3].

The main technical applications of the problem in the mixed convection heat transfer in closed canals are in the design and analysis of heat exchangers, mechanical, electrical, electronics, and many others practical's have taken a new revolution as it ventures into the period. For example, a heat exchanger problem which mainly concerns with food or chemical industries, when products to be treated may exhibit complex rheological behaviour, such as concentrated fruit purees, fruit juices, emulsions and polymeric melts, which present high apparent viscosity. The tubular heat exchangers are one of the commonest types of heat exchangers in the food industry and their typical areas of application are in the sterilization and pasteurization. On the other hand, the concentric and eccentric annular geometry is widely employed in the field of heat exchangers, as it is used in numerous heat transfers and fluid flow devices involving two fluids. One fluid flows through the inner tube while the other flows through the annular passage between the two tubes. For example, gas-cooled electrical cables, heat exchangers designed for chemical processes require the consideration of mixed convection in an annular flow. Cooling of nuclear fuel rods is another example where the results for the buoyancy-influenced convection in an annulus are useful [4].

Several attempts in this field have been completed to formulate appropriate effective thermal conductivity and dynamic viscosity of nanofluid [5]. Teng et al. [6] have measured the effects of temperature, nanoparticles size and weight fraction on the thermal conductivity of Al_2O_3–Water nanofluid. They compared their results with numerical results and proposed a significant correlation for thermal conductivity, which depends on temperature, nanoparticles size and weight fraction. Das et al. [7] have investigated a water–Al_2O_3 mixture experimentally and found that increasing temperature increases the effective thermal conductivity remarkably while the dynamic viscosity decreases. Yu et al. [8] measured that the thermal conductivity of ZnO-EG nanofluid. They establish that the enhanced value of 5.0 vol% ZnO-EG nanofluid is 26.5%, well beyond the values given by the existing classical models for the solid liquid mixture, and it is consistent with the prediction values by the combination of the aggregation mechanism with the Maxwell and Bruggeman models.

The single phase approach is simpler and requires less computational time, which assumes that the fluid phase and particles are in thermal equilibrium and move with the same velocity. But using appropriate expressions which calculate the properties of single phase nanofluid are beneficial and notable. However, the single phase approach has been used in many theoretical studies of convective heat transfer with nanofluids [9]. Hence, the properties of nanofluids are not completely specified, and there are not good expressions for predicting nanofluid mixture, generally the single phase numerical prediction are in good agreement with the experimental results.

Some researchers have considered the application of nanofluids in an annulus [10,11]. Abu-Nada [10] has studied single phase Al_2O_3–water nanofluid flow in an annulus. Different viscosity and thermal conductivity models are used to evaluate heat transfer enhancement in the annulus by his work. Izadi et al. [11] have also investigated laminar forced convection of a nanofluid consisting of Al_2O_3 and water numerically in a two dimensional annulus with single phase approach. The tubes of elliptic cross section have drawn particular attention since they were found to create less resistance to the cooling fluid which results in less pumping power [12]. Velusamy and Garg [13] have studied mixed and forced convection fluid flow in ducts with elliptic and circular cross sections. They found that irrespective of the value of the Rayleigh number, the ratio of friction factor during mixed convection to the corresponding value during forced convection is low in elliptical ducts compared to that in a circular duct as well as the ratio of Nusselt number to friction factor is higher for elliptic ducts compared to that for a circular duct. Despite the fact that these secondary flow in elliptical ducts is very small compared to the stream wise bulk flow, secondary motions play a significant role by cross-stream transferring momentum, heat and mass. On the other hand, the main advantage of using elliptic ducts than circular ducts is the increase of heat transfer coefficient [14]. Hence, heat transfer enhancement in these devices is essential, nanofluids usage can be play effective roles to increase heat transfer coefficient.

It is obvious from the above literature review that the heat transfer augmentation of laminar mixed convection flow using nanofluids in an elliptic annulus with constant heat flux seems not to have been investigated in the past, and this has motivated the current work. In addition, most of the previous research on elliptic annulus involved conventional fluids (not nanofluids) and there is a very little work reported in the open literature that involved nanofluids in an elliptic annulus. However, there is no previous research involved the usage of nanofluid in an elliptic annulus. The present study examines 3D laminar mixed convective heat transfer in an elliptic annulus with uniform heat flux by using different types of nanofluids, different nanoparticle volume fractions, and different nanoparticle diameters are dispersed in different base fluids (water, glycerine, engine oil and ethylene glycol). This investigation covers Reynolds number in the range of 200 to 1000 and particle diameters range from 20 to 80 nm. Different types of nanofluids and different volume fractions ranged from 0% to 4%. Results of interests such as Nusselt number, velocity profile and temperature contours for laminar mixed convection heat transfer in an elliptic annulus are reported to illustrate the effect of nanofluids on these parameters.

2. Mathematical modeling

2.1. Physical model

The physical model of the test section mainly consists of two concentric horizontal cylinders are used to form an annular space ranging from an elliptical tube placed at the center of a circular cylinder. The outer cylinder was made from

aluminium of 50.8 mm outer diameter, 1 mm thickness, and 500 mm length. The inner elliptic cylinder was made of aluminium with a major radius (r_2) of 9 mm and a length of 500 mm that had an axis ratio ($r_1/r_2=1/3$). Pure water, various nanoparticles and various base fluids are selected as the working fluid and the thermo physical properties assumed to be temperature independent. The thermo-physical properties of water and nanoparticle materials which used for simulation are shown in Table 1. The internal wall of the annular space (elliptic tube surface) was maintained under constant heat flux (q_h). Whereas the external wall of the annular space (circular cylinder surface) was kept isothermally at a constant temperature (T_c). The schematic diagram of the annular space under consideration and coordinate system are shown in Fig. 1.

2.2. Geometry and the governing equations

The three-dimensional Navier–Stokes and energy equations were used to describe the flow and heat transfer in the annuals. Fig. 2 presents the computational grid; heat is transferred between the fluids through the wall which is separating them. Numerous assumptions were made on the operating conditions of the annulus: (i) the annulus operates under steady-state conditions and three-dimensional; (ii) the nanofluid is Newtonian and incompressible; (iii) fluid is in single phase and the flow is laminar; (iv) the external heat transfer effects are ignored; (v) the outer walls of the annulus are adiabatic; and (vi) constant thermophysical properties are considered for the nanofluid, except for the density variation in the buoyancy forces, determined by using the Boussinesq approximation where the approximation is applicable for sufficiently small temperature deference between the inner and outer cylinders.

The governing equations for flow and heat transfer in the annulus are as follows [15]:

Continuity equation:

$$\frac{\partial \rho}{\partial t}+\nabla \times (\rho V) = 0 \tag{1}$$

Momentum equation:

$$\rho\frac{D\mathbf{V}}{Dt} = \nabla \times \boldsymbol{\tau}_{\mathbf{ij}} - \nabla p + \rho\mathbf{F} \tag{2}$$

Table 1
The thermophysical properties of different nanoparticles and different base fluids at $T=300$ K.

Thermophysical Properties	Al_2O_3	CuO	SiO_2	ZnO	Water	Glycerine	Engin oil	EG
ρ (kg/m^3)	3600	6500	2200	5600	996.5	1259.9	884.1	1114.4
Cp (J/kg K)	765	533	745	495.2	4181	2427	1909	2415
k (W/m K)	36	17.65	1.4	13	0.613	0.286	0.145	0.252
μ(N s/m^2)	–	–	–	–	1×10^{-3}	0.799	0.486	0.0157
β (1/K)	5.8×10^{-6}	4.3×10^{-6}	5.5×10^{-6}	4.31×10^{-6}	2.75×10^{-4}	4.8×10^{-4}	7×10^{-4}	6.5×10^{-6}

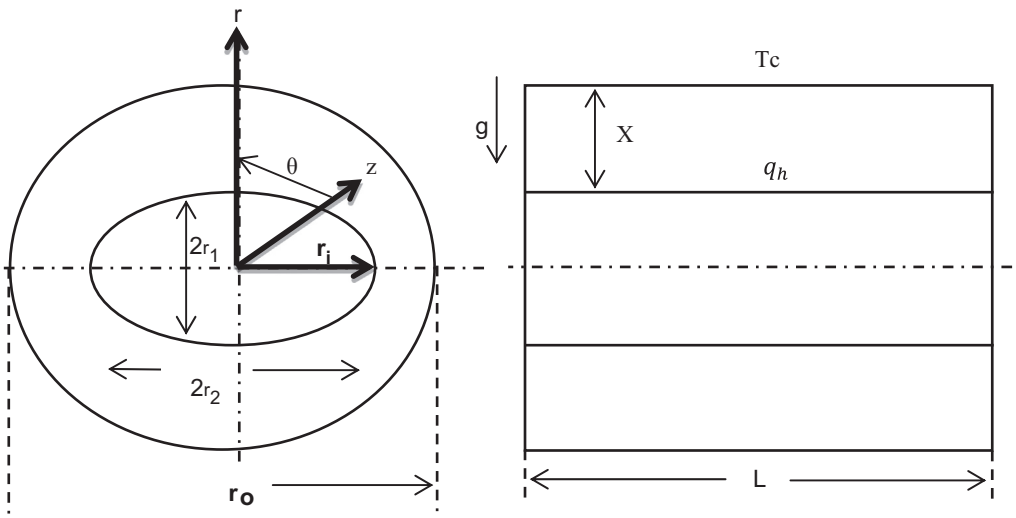

Fig. 1. Schematic diagram of the computational domain of annulus.

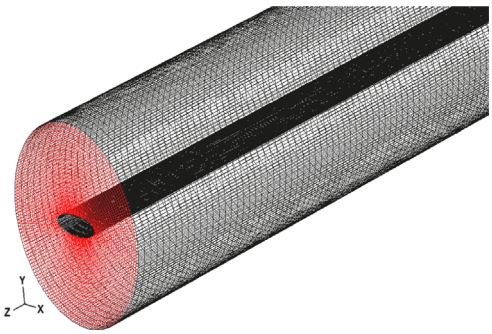

Fig. 2. Computational grid of an elliptic annulus.

Energy equation:

$$\rho\frac{De}{Dt}+\rho(\nabla\times\mathbf{V})=\frac{\partial Q}{\partial t}-\nabla\times\mathbf{q}+\mathbf{\Phi} \tag{3}$$

where **V** is the fluid velocity vector, **F** is the body forces, **q** represents heat transfer by conduction and **Φ** is the dissipation term. These governing equations along with the given boundary conditions are solved to obtain the fluid temperature distribution and pressure drop along the annulus. These data were then used to examine the thermal and flow fields along the annulus.

2.3. Boundary conditions

At the elliptic inlet, different velocities depending on the values of Reynolds number were used, and the outlet temperature was taken as Tin=300 K. The constant heat flux used was 5000 W/m^2 to heat up the inside walls. At the domain outlet the flow and heat transfer are assumed to be fully developed. The boundary condition can be expressed as follows:

- At the inlet of annulus ($z=0$ and $r_i \le r \le r_o$):

$$u_r = u_\theta = u_z = 0, \quad \text{and} \quad T = T_i \tag{4}$$

- At the fluid wall interface: ($r=r_i$ and $0 \le z \le L$)

$$u_r = u_\theta = u_z = 0, \quad \text{and} \quad q_{w,i} = -k_{\text{eff}}\frac{\partial T}{\partial r}\bigg|\, r = ri \tag{5}$$

- At the outlet of annulus ($z=L$ and $r_i \le r \le r_o$): $p=p_0$ and an overall mass balance correction is applied.

2.4. Nanofluids thermophysical properties

The thermophysical properties of pure water, various nanoparticles and various base fluids which are density, heat capacity, effective dynamic viscosity, effective thermal conductivity and thermal expansion coefficient are given in Table 1. Meanwhile the nanofluids thermophysical properties for 20 nm particle size and volume fraction of 0–4% for various nanoparticles (Al_2O_3, ZnO, SiO_2 and CuO) are given in Tables 2 and 3. These properties are calculated using the following equations:

Effective thermal conductivity [16]

$$k_{\text{eff}} = k_{\text{static}} + k_{\text{Brownian}} \tag{6}$$

$$k_{\text{static}} = k_{bf}\left[\frac{(k_{np}+2k_{bf})-2\phi(k_{bf}+2k_{np})}{(k_{np}+2k_{bf})+\phi(k_{bf}+2k_{np})}\right] \tag{7}$$

where k_{np} and k_{bf} are the thermal conductivity of the nanoparticle and the base fluid, respectively.

Thermal conductivity due to the Brownian motion presented by [17] as:

$$k_{\text{Brownian}} = 5\times10^4\beta\phi\rho_{bf}C_{pbf}\sqrt{\frac{kT}{2\rho_{np}R_{np}}}f(T,\phi) \tag{8}$$

Table 2
The values of β for different particles with its boundary conditions [17].

Type of particles	B	Concentration	Temperature
Al_2O_3	$8.4407(100\phi)^{-1.07304}$	$1\% \le \phi \le 10\%$	$298\ K \le T \le 363\ K$
CuO	$9.881(100\phi)^{-0.9446}$	$1\% \le \phi \le 6\%$	$298\ K \le T \le 363\ K$
SiO_2	$1.9526(100\phi)^{-1.4594}$	$1\% \le \phi \le 10\%$	$298\ K \le T \le 363\ K$
ZnO	$8.4407(100\phi)^{-1.07304}$	$1\% \le \phi \le 7\%$	$298\ K \le T \le 363\ K$

Table 3
Thermophysical properties of nanofluids used in this study.

Properties	Water base fluid, $\phi = 0.04$, $dp = 20$ nm			
	ZnO	Al_2O_3	CuO	SiO_2
Effective density, ρ_{eff} (kg/m^3)	1115.44	1216.64	1044.64	1180.64
Effective specific heat, Cp_{eff} (J/kg K)	3694.68	3401.96	3888.015	3481.702
Effective thermal conductivity, k_{eff} (W/m K)	0.68310	0.73040	0.636744	0.71542
Effective dynamic viscosity, μ_{eff} (N s/m^2)	0.00139	0.00139	0.00139	0.00139
Effective thermal expansion coefficient $\beta(1/k)$	2.372×10^{-4}	1.892×10^{-5}	2.529×10^{-4}	1.024×10^{-5}

$$f(T,\phi) = (0.028217\phi + 0.003917)\frac{T}{T_o} + (0.030669\phi - 0.00391123) \tag{9}$$

where k is the Boltzman constant, T is the fluid temperature and T_0 is the reference temperature. The term of $f(T,\varnothing)$ is a function of temperature and particle volume fraction. The correlation of β is a function of the liquid volume that travels with a particle material expressed in Table 2 as it is given by Vijjha [17]. The effective dynamic viscosity is given as [18]:

$$\frac{\mu_{eff}}{\mu_{bf}} = \frac{1}{1 - 34.8(d_{np}/d_{bf})^{-0.3}\phi^{1.03}} \tag{10}$$

where $d_{bf} = [6M/N\pi\rho_{bf}]^{1/3}$ μ_{eff} and μ_{bf} are the effective dynamic viscosity of nanofluid and dynamic viscosity of the base fluid, respectively, d_{np} is the nanoparticle diameter, d_{bf} is the base fluid equivalent diameter and ϕ is the nanoparticle volume fraction. M is the molecular weight of the base fluid, N is the Avogadro number $= 6.022 \times 10^{23}$ mol^{-1} and ρ_{fo} is the mass density of the base fluid calculated at temperature $T_0 = 293$ K. The effective density is given as [18]:

$$\rho_{eff} = (1-\phi)\rho_{bf} + \phi\rho_s \tag{11}$$

where ρ_{eff} and ρ_{bf} are the nanofluid and base fluid densities, respectively, and ρ_s is the density of nanoparticle. The effective specific heat at constant pressure of the nanofluid $(C_p)_{eff}$ is computed using the following equation [18]:

$$(Cp)_{eff} = \frac{(1-\phi)(\rho Cp)_{bf} + \phi(\rho Cp)_s}{(1-\phi)\rho_{bf} + \phi\rho_s} \tag{12}$$

where Cp_s and Cp_{bf} are the heat capacity of solid particles and base fluid, respectively. Properties of nanofluids at volume fraction 4% used in this study are available in Table 3.

The Reynolds number and the Nusselt number are expressed by the following relations [19]:

$$\mathrm{Re} = \frac{u_{av}D_h}{\nu} \tag{13}$$

$$Nu = \frac{hD_h}{k} \tag{14}$$

2.5. Numerical parameters and procedures

The numerical computations were carried out by solving the governing conservation along with the boundary conditions using the finite volume method(FVM) with the aid of commercial software(FLUENT©). It is based on the control volume method; COUPLED algorithm is used to deal with the problem of velocity and pressure coupling. The pressure staggering option (PRESTO) scheme is used to solve pressure equations. SIMPLE algorithm is used to solve the flow field inside an annulus. The diffusion term in the momentum and energy equations is approximated by the first-order central difference which gives a stable solution. In addition, a first-order upwind differencing scheme is adopted for the convective terms [20]. The numerical model was developed in the physical domain, and dimensionless parameters were calculated from the

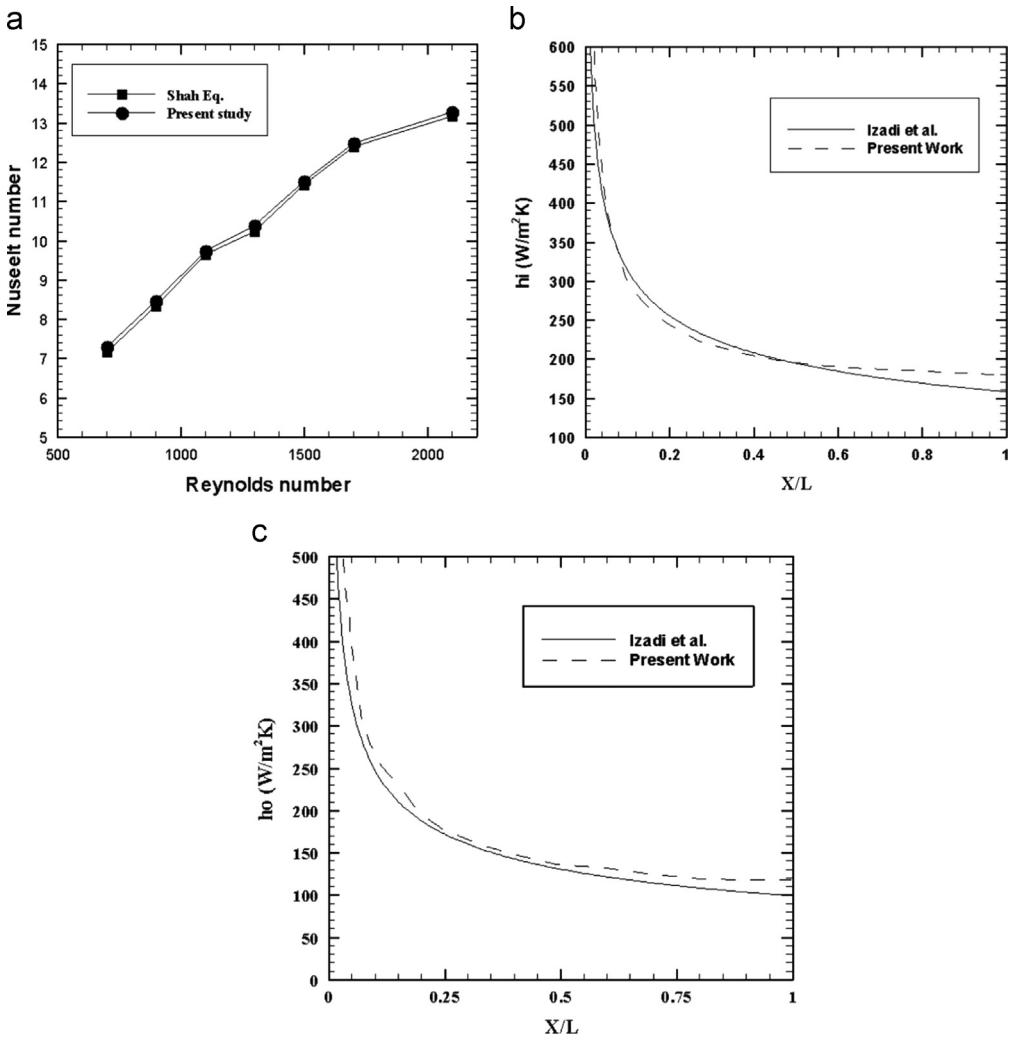

Fig. 3. Comparison of the heat transfer coefficient at (b) inner wall and (c) outer wall, respectively, with published numerical results carried out by Izadi et al. at $Re=900$, $\emptyset=0.03$, $q_i/q_o=1$, $dp=25$ mm [11].

computed velocity and temperature distributions. The residual sum for each of the conserved variables is computed and stored at the end of each iteration. The convergence criterion required that the maximum relative mass residual based on the inlet mass be smaller than 1×10^{-6}.

2.6. Grid testing and code validation

The computational domain resulted from the subtraction of the elliptical cylinder section from the circular cylinder section. The grid is made up of triangular elements to improve the quality of the numerical prediction near the curved surfaces as shown in Fig. 3. Four different sets of the grid sizes were imposed to the geometry and simulated by calculating the Nusselt number at $Re=1000$. The four grids sizes are $40\times10\times100$, $20\times10\times200$, $50\times10\times200$ and $40\times30\times100$ show no much difference in the values of Nusselt number. Thus, the grid size of $40\times10\times100$ is selected in this study as it is found to provide a more stable grid independent solution. The code validation was done based on the geometry and boundary conditions which were used by Izadi et al. [11]. They studied the thermal characteristics of laminar mixed convection flow in an elliptic annulus with constant heat flux boundary condition. In this case, the results of the Nusselt number variation were compared with the predictions of the following well-known Shah equation for laminar flows under the constant heat flux boundary condition [11] as shown in Fig. 3a. To validate the accuracy of the numerical solutions, the Nusselt number (Nu) of the elliptic annular is compared with the theoretical data. It is clearly seen that the deviation between the numerical results and the theoretical data is 5% by Izadi et al. [11] as shown in Fig. 3b and c. Therefore, the present numerical prediction ns have reasonable accuracy.

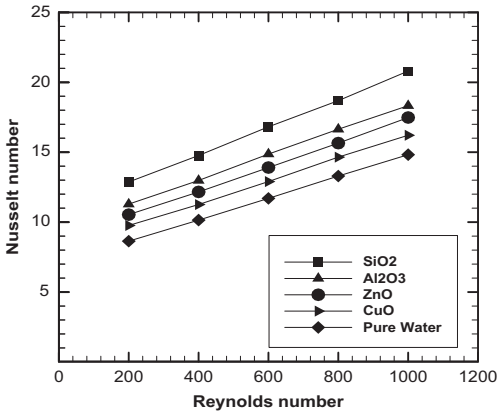

Fig. 4. The effect of different nanofluids types at different Reynolds numbers for Nusselt number.

3. Results and discussion

The simulations are performed of laminar heat transfer and fluid flow through an elliptic annulus with four different types of nanofluids such as Al_2O_3, CuO, SiO_2 and ZnO with pure water as a base fluid. Five values of Reynolds number were used in the range of $200 \leq Re \leq 1000$ with four nanoparticles volume friction in the range of $0 \leq \phi \leq 0.04$ and nanoparticles diameter in the range of $20\ \text{nm} \leq dp \leq 80\ \text{nm}$. The effects of particle type, volume fraction, particle diameter, Reynolds number and different base fluids on the Nusselt number and friction factor are analyzed and discussed in this section.

3.1. The effect of different types of nanoparticles

Four different types of nanoparticles such as Al_2O_3, CuO, SiO_2 and ZnO and pure water as a base fluid are used. The nanoparticle type affects the nanofluid properties which in turn affect the heat transfer performance. The Nusselt number for different values of Reynolds number and different nanofluids are shown in Fig. 4. It can be obviously seen that SiO_2 nanofluid has the highest surface Nusselt number, followed by Al_2O_3, ZnO, and CuO, respectively. This is because SiO_2 has the lowest thermal conductivity than other nanofluids, but higher than water and has the highest average velocity among other fluids due to its lowest density compared with the others. The surface Nusselt number increases significantly as Reynolds number increases for the four nanofluids types. It is less dense and this property enables the particle to move rapidly in the annulus tube and it characterizes the main reason to give high heat transfer coefficient. In general, the value of Nusselt number is inversely proportional to the value of thermal conductivity of that particular fluid.

3.2. The effect of different nanoparticles on the velocity and temperature profiles

It is pointed out that increasing the radial and longitudinal velocity has a significant effect on increasing the annulus tube heat transfer rate. In order to explain the effect of nanofluid velocity on heat transfer rate, the CFD predicted the velocity magnitudes relating to the type of nanofluid and compared for $Re = 1000$ as shown in Fig. 5(a). It can be clearly seen that SiO_2 being the nanofluid with the lowest density shows the highest amount of pressure drop due to higher velocity followed by CuO, Al_2O_3, ZnO, and water. This can be the reason of more heat transfer rate obtained.

For $Re = 1000$, $\phi = 0.04$, $dp = 20$ nm to different nanoparticle types of the heat transfer patterns in annulus zone via the temperature contour are demonstrated in Fig. 5(b). In this case, the lower surface temperature corresponds to the higher convective heat transfer. The results indicate that the maximum heat transfer rate is found around the elliptical inner pipe and diminishes along the radial direction. However, the higher convective heat transfer (lower surface temperature) obtained from the usage of CuO nanofluid. This means that the random movements of CuO nanoparticles enhance the thermal dispersion of the flow better than water and other nanoparticles. It can be clearly seen that the present results of this case correspond with another study.

3.3. The effects of nanoparticles volume fraction, nanoparticle diameter and base fluid

The effect of nanoparticles volume fraction on the average Nusselt number with different Reynolds number at $dp = 20$ nm is depicted in Fig. 6(a). At a given Reynolds number, it can clearly seen that the average Nusselt number increases as the volume fraction of the nanoparticles increases due to improve the thermal conductivity of the nanofluid. It can also be seen at particular volume fraction; the average Nusselt number increases with increasing Reynolds number due to increases the temperature gradient at the wall. This is because as the volume fraction increases, irregular and random movements of the

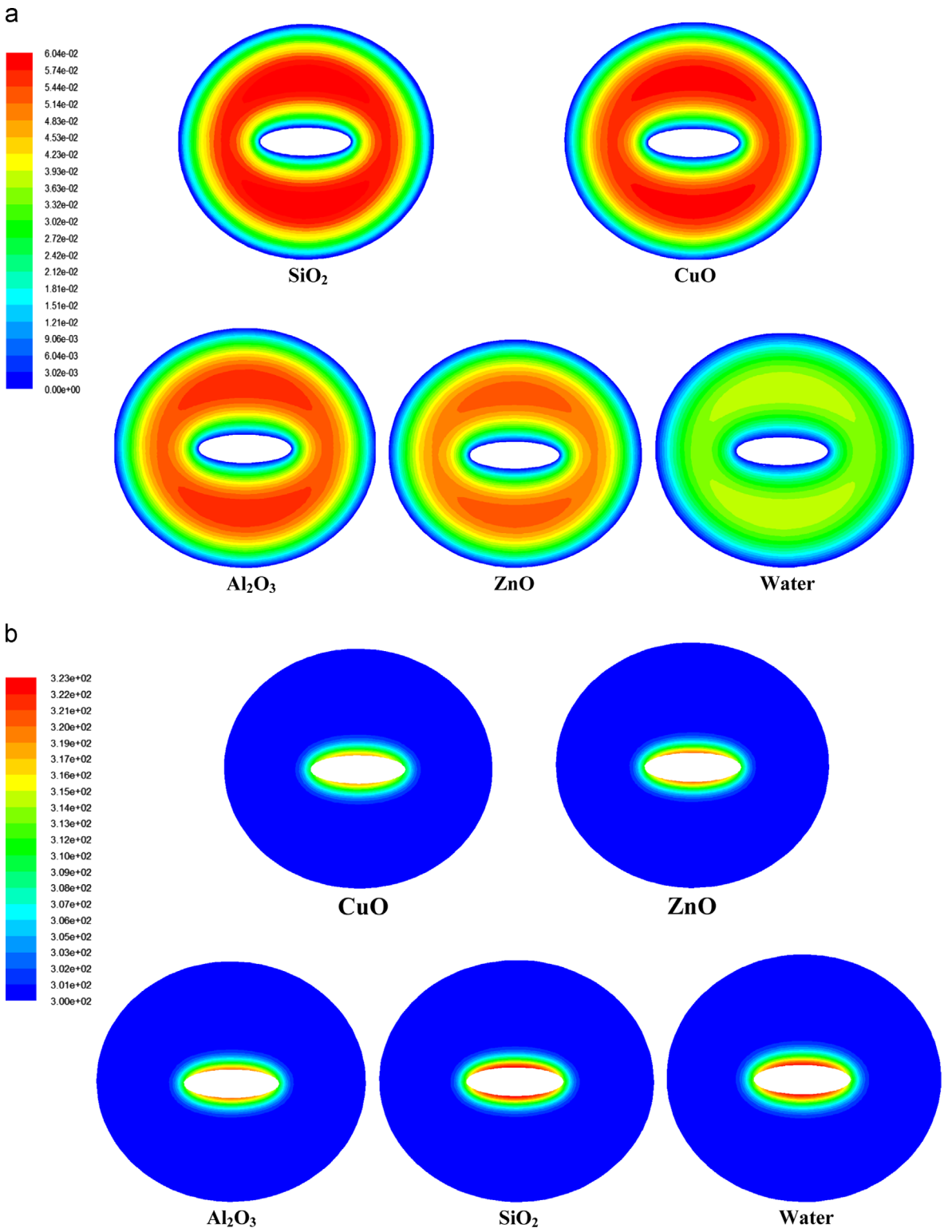

Fig. 5. (a) The contours of velocity of different nanoparticle for $Re=1000$, $\phi=0.04$, $dp=20$ nm in the annulus tube. (b) The contours of temperature of different nanoparticle types. For $Re=1000$, $\phi=0.04$, $dp=20$ nmin the annulus tube.

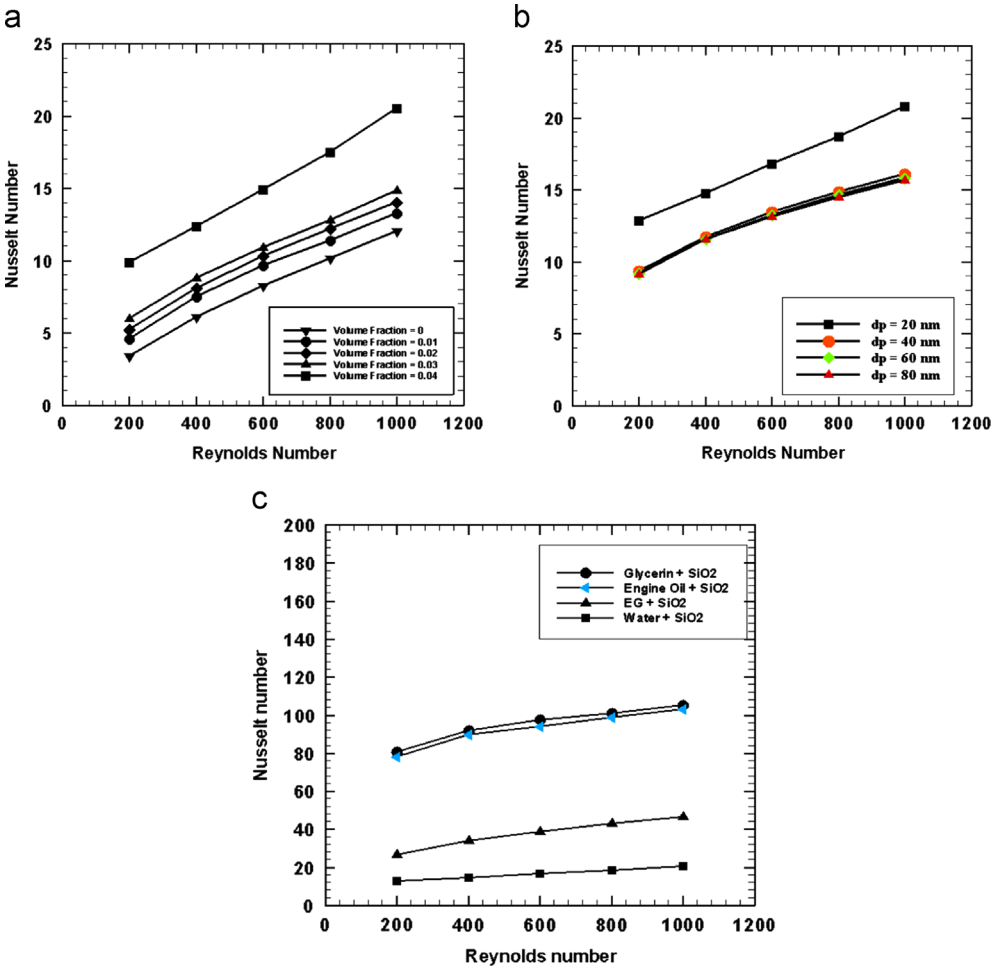

Fig. 6. The effect of (a) different volume fractions of nanoparticles at different Reynolds number for Nusselt number. (b) Different nanoparticles diameters at different Reynolds number for Nusselt number. (c) Different base fluids at different Reynolds number for Nusselt number.

particles increases the energy exchange rates in the fluid with a penalty on the wall shear stress and consequently augment the thermal dispersion of the flow.

Fig. 6(b) shows the effect of the nanoparticles diameter on the average Nusselt number with different Reynolds numbers at 4% volume fraction of the SiO_2–water nanofluid. According to this figure, it is found that the average Nusselt number increases as the particle diameter decreases. This is because the surface area per unit volume increases with decreasing in the particle diameter. In addition, the Brownian motion is higher for the smaller particles. Parsazadeh et al. [21] also observed that the average Nusselt number increases as the particle diameter decreases.

The effect of different types of base fluids on the Nusselt number versus the Reynolds number is presented in Fig. 6(c). It can obviously be seen that SiO_2-glycerine has the highest value of Nusselt number while SiO_2–water has the lowest value of Nusselt number. This is because glycerine has the highest dynamic viscosity in nature compared to other base fluids and SiO_2 particles are mixed properly in glycerine which contributes to increase the thermal transport capacity of the mixture which in turn increases the Nusselt number.

4. Conclusions

Numerical simulations of laminar mixed convection heat transfer using nanofluids such as Al_2O_3, CuO, SiO_2 and ZnO as the working fluids in an elliptic annulus with uniform heat flux were reported. The emphasis is given on the heat transfer enhancement resulting from various parameters, which include nanofluid types, volume fraction of nanoparticle, nanoparticle diameter and base fluid type. The governing equations were solved utilizing finite volume method with certain assumptions and appropriate boundary conditions.

The results were obtained through the numerical simulation that gives the highest Nusselt number. It is clearly observed that the best setting of parameters that gave the best heat transfer enhancement through the elliptic annulus were by using SiO_2 (silicon dioxide) as the working fluid with percentage of concentration of 4%, diameter of particle (*dp*) of 20 nm, using

Reynolds number of 1000. The Nusselt number is remarkably increased with the increase of nanoparticle volume fraction and Reynolds number; however, it is decreased with the increase of nanoparticles diameter. Results reveal that glycerine–SiO_2 gives the highest Nusselt number followed by engine oil–SiO_2, EG-SiO_2, respectively, while water–SiO_2 gives the lowest Nusselt number.

References

[1] Joye D. Pressure drop correlation for laminar, mixed convection, aiding flow heat transfer in a vertical tube. Int J Heat Fluid Flow 2003;24(2):260–6.
[2] Mohammed HA. Laminar mixed convection heat transfer in a vertical circular tube under buoyancy-assisted and opposed flows. Energy Convers Manage 2006;49(8):2006–15.
[3] MokhtariMoghari R, Akbarinia A, Shariat M, Talebi F, Laur R. Two phase mixed convection Al_2O_3–water nanofluid flow in an annulus. Int J Multiphase Flow 2011;37(6):585–95.
[4] Islam N, Gaitonde UN, Sharma GK. Mixed convection heat transfer in the entrance region of horizontal annuli. Int J Heat Mass Transfer 2001;44(11):2107–20.
[5] Wang BX, Zhou LP, Peng XF. A fractal model for predicting the effective thermal conductivity of liquid with suspension of nanoparticles. Int J Heat Mass Transfer 2003;46(14):2665–72.
[6] Teng T-P, Hung Y-H, Teng T-C, Mo H-E, Hsu H-G. The effect of alumina/water nanofluid particle size on thermal conductivity. Appl Therm Eng 2010;30(14–15):2213–8.
[7] Das SK, Putra N, Thiesen PW, Roetzel R. Temperature dependence of thermal conductivity enhancement for nanofluids. J Heat Transfer 2003;125(4):567–74.
[8] Yu W, Xie H, Chen L, Li Y. Investigation of thermal conductivity and viscosity of ethylene glycol based ZnO nanofluid. Thermochim Acta 2009;491:92–6.
[9] Talebi F, Mahmoudi AH, Shahi M. Numerical study of mixed convection flows in a square lid-driven cavity utilizing nanofluid. Int Commun Heat Mass Transfer 2010;37:79–90.
[10] Abu-Nada E. Effects of variable viscosity and thermal conductivity of Al_2O_3–water nanofluid on heat transfer enhancement in natural convection. Int J Heat Fluid Flow 2009;30(4):679–90.
[11] Izadi M, Behzadmehr A, Jalali-Vahida D. Numerical study of developing laminar forced convection of a nanofluid in an annulus. Int J Therm Sci 2009;48:2119–29.
[12] Velusamy K, Garg VK, Vailyanathan G. Fully developed flow and heat transfer in semi-elliptical ducts. Int J Heat Fluid Flow 1995;16:145–52.
[13] Velusamy K, Garg VK. Laminar mixed convection in vertical elliptic ducts. Int J Heat Mass Transfer 1996;39(4):745–52.
[14] Sakalis VD, Hatzikonstaninoi PM, kafousias N. Thermally developing flow in elliptic ducts with axially variable wall temperature distribution. Int J Heat Mass Transfer 2002;45:25–35.
[15] Ashgriz, N., Mostaghimi, J., An introduction to computational fluid dynamics. In: Fluid flow handbook, McGraw-Hill Handbooks, New York, NY; 2002 (Chapter 20).
[16] Ghasemi B, Aminossadati S. Brownian motion of nanoparticles in a triangularenclosure with natural convection. Int J Therm Sci 2010;49:931–40.
[17] Vajjha RS, Das DK. Experimental determination of thermal conductivity of three nanofluids and development of new correlations. Int J Heat Mass Transfer 2009;52:4675–82.
[18] Corcione M. Heat transfer features of buoyancy-driven nanofluids inside rectangular enclosures differentially heated at the sidewalls. Int J Therm Sci 2010;49:1536–46.
[19] Eiamsa-ard S, Promvonge P. Thermal characteristics of turbulent rib-grooved channel flows. Int Commun Heat Mass Transfer 2009;36:705–11.
[20] Patankar SV. Numerical heat transfer and fluid flow. New York, NY: Hemisphere; 1980.
[21] Parsazadeh M, Mohammed HA, Fathinia F. Influence of nanofluid on turbulent forced convective flow in a channel with detached rib-arrays. Int Commun Heat Mass Transfer 2013;46:97–105.